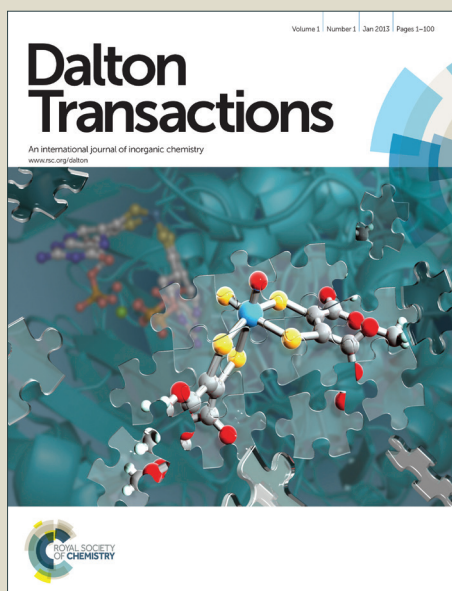


# Dalton Transactions

Accepted Manuscript



This article can be cited before page numbers have been issued, to do this please use: M. Lemaire, A. J. Lough and D. Dinsdale, *Dalton Trans.*, 2015, DOI: 10.1039/C5DT00743G.



This is an *Accepted Manuscript*, which has been through the Royal Society of Chemistry peer review process and has been accepted for publication.

*Accepted Manuscripts* are published online shortly after acceptance, before technical editing, formatting and proof reading. Using this free service, authors can make their results available to the community, in citable form, before we publish the edited article. We will replace this *Accepted Manuscript* with the edited and formatted *Advance Article* as soon as it is available.

You can find more information about *Accepted Manuscripts* in the [Information for Authors](#).

Please note that technical editing may introduce minor changes to the text and/or graphics, which may alter content. The journal's standard [Terms & Conditions](#) and the [Ethical guidelines](#) still apply. In no event shall the Royal Society of Chemistry be held responsible for any errors or omissions in this *Accepted Manuscript* or any consequences arising from the use of any information it contains.

## ARTICLE

## Structure and magnetic properties of an unusual homoleptic iron(III) thiocyanate dimer

Cite this: DOI: 10.1039/x0xx00000x

D. R. Dinsdale,<sup>a</sup> A. J. Lough<sup>b</sup> and M. T. Lemaire<sup>\*a</sup>,Received 00th January 2012,  
Accepted 00th January 2012

DOI: 10.1039/x0xx00000x

www.rsc.org/

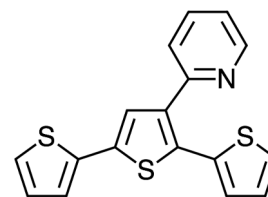
We describe the structural and variable temperature magnetic susceptibility properties of an unusual homoleptic bimetallic iron(III) thiocyanate tetraanion. This work represents the first structurally characterized *bis*( $\mu$ -1,3-thiocyanato) dimer of iron(III). A weak antiferromagnetic exchange interaction is observed between the two iron(III) ions, which is supported by broken symmetry density functional theory (dft) calculations.

## Introduction

The thiocyanate (SCN<sup>-</sup>) anion has played an important role in the development of the field of transition metal coordination chemistry. There exist a wide array of complexes containing the ambidentate thiocyanate as a terminally bound ligand (both N- or S- bound), as a bridging ligand (both  $\mu$ -1,3 end-on-end and  $\mu$ -1,1 end-on bridging modes) and as a counteranion.<sup>1</sup> The thiocyanate ligand has played a significant role in the development of complexes that exhibit spin-crossover and in other molecule-based magnetic materials, providing itself as an intermediate field ligand to observe the thermal reversibility of spin states and as a magnetic coupling unit when bridging metal centers together in polynuclear complexes.<sup>2-6</sup>

In a previous study we had used in situ prepared “Fe(NCS)<sub>2</sub>” to generate 6-coordinate iron(II) spin-crossover complexes containing two equivalents of a bidentate ligand bearing one or two thiophene substituents, and in one case we were able to electropolymerize the complex to produce a conducting metallopolymer film.<sup>7</sup> We were eager to explore other polymerizable bidentate ligands in this regard to prepare Wolf Type 2 conducting polymers where the iron ion is coordinated directly to the polymer backbone, rather than tethered to the chain.<sup>8</sup> Our target ligand in this strategy **1** was previously reported<sup>9</sup> and we envisioned possible coordination of the 2-pyridyl donor N atom and thiophene S atom to “Fe(NCS)<sub>2</sub>” to produce similar complexes as previously reported.<sup>7</sup> However, rather than obtaining the anticipated 6-coordinate iron(II) complexes, we obtained a most unusual ionic complex containing a completely homoleptic thiocyanate iron(III) dimer. To our knowledge this is the first such reported material and the first bimetallic iron(III) complex with bridging  $\mu$ -1,3 thiocyanate ligands. Herein we report the structure of this

complex obtained by single crystal X-ray diffraction, as well as its spectroscopic and variable temperature magnetic susceptibility properties, which indicate weak antiferromagnetic interactions between the iron(III) ions supported by broken symmetry density functional theory (DFT) calculations.

Fig 1. Structure of **1** indicating possible N,S bidentate donor atoms

## Experimental

## Materials and methods

## GENERAL PROCEDURES

All reagents were commercially available and used as received unless otherwise stated. Deaerated and anhydrous solvents were obtained from a Puresolve PS MD-4 solvent purification system. <sup>1</sup>H/<sup>13</sup>C-NMR spectra were recorded on a Bruker Avance 400 MHz spectrometer using deuterated solvents. FT-IR spectra were recorded on a Shimadzu IRAffinity spectrometer as KBr discs. UV-Vis measurements were recorded on a Shimadzu 3600 UV-Vis-NIR spectrophotometer in CH<sub>2</sub>Cl<sub>2</sub> solution using quartz cuvette cells. Elemental analyses were carried out by Canadian Microanalytical Services, LTD., Delta, BC, Canada. LC-MS experiments were recorded on an Agilent 1260 Infinity liquid chromatograph/6530 accurate mass Q-TOF in high resolution

mode with 70:30 acetonitrile/water using positive mode electrospray ionization (HPLC grade solvents). Differential Pulse (DP) voltammetry experiments were performed with a Bioanalytical Systems Inc. (BAS) Epsilon electrochemical workstation. Compound **2** was dissolved in anhydrous solvent ( $\text{CH}_2\text{Cl}_2$ ), and then deaerated by sparging with  $\text{N}_2$  gas for 10–15 min in a low-volume cell. Solution concentrations were approximately  $10^{-3}$  M in analyte containing approximately 0.5 M supporting electrolyte ( $\text{Bu}_4\text{NPF}_6$ ). A typical three-electrode set-up was used including a glassy carbon working electrode, Ag/AgCl reference electrode, and a platinum wire auxiliary electrode. The scan rate for all DP experiments was 25 mV/s. Variable temperature magnetic susceptibility measurements for **2** was recorded on an MPMS SQUID magnetometer at an external magnetic field of 2000 Oe over a temperature range of 2–300 K. The sample was weighed into a gel cap and diamagnetic contributions were calculated using Pascal's constants.

#### COMPUTATIONAL DETAILS

Single point energy DFT calculations were performed on the tetra-anion of **2** based on the coordinates obtained from the single crystal X-ray diffraction data using the Gaussian09 (Revision D.01) package<sup>10</sup> using the B3LYP hybrid functional<sup>11,12</sup> and the def2-TZVP<sup>13</sup> basis set on all atoms. Tight SCF convergence criteria were used for all calculations. The program Chemissian<sup>14</sup> was used for the preparation of the spin density distribution figure.

#### Synthetic procedures

**3'-(pyrid-2-yl)-2,2':5',2''-terthiophene (1).** Under a  $\text{N}_2$  atmosphere a pre-dried Schlenk flask was charged with  $\text{Pd}(\text{PPh}_3)_4$  (0.15 g, 0.13 mmol, 5.6 mol%) in dry toluene (10 mL). 3'-bromo-2,2':5',2''-terthiophene (0.74 g, 2.3 mmol) was dissolved in dry toluene (15 mL) and was added to the Schlenk followed by 2-pyridylzinc bromide solution (7.0 mL of 0.50 M THF solution, 3.5 mmol) and the mixture was heated to 100 °C for 72 h. The cooled reaction contents were stirred with a 0.5 M EDTA solution (60 mL) containing 1.0 M  $\text{K}_2\text{CO}_3$  (60 mL) for 0.5 hr and then extracted with diethyl ether ( $3 \times 50$  mL). The combined organic extracts were dried over  $\text{MgSO}_4$ , filtered and rotovaped to dryness. The crude product was chromatographed over silica gel, eluting with 15:1 hexanes/ethyl acetate to produce a yellow oil. Yield, 0.36 g (48%). Spectroscopic data was consistent with a previous reported synthesis of **1**.<sup>9</sup> HR-MS (ESI+): Calc'd for  $\text{C}_{17}\text{H}_{12}\text{NS}_3\text{C}$   $m/z$  326.0126  $[\text{MH}^+]$ , found 326.0124.  $^1\text{H}$  NMR ( $\text{CDCl}_3$ , 400 MHz):  $\delta$  8.74 (1H, d,  $J = 4.8$  Hz), 7.70 (1H, td,  $J_1 = 7.7$  Hz and  $J_2 = 1.8$  Hz), 7.62 (1H, s), 7.40 (1H, d,  $J = 7.9$  Hz), 7.34–7.22 (4H, m), 7.09 (1H, d,  $J = 3.2$  Hz), 7.08–7.00 (m, 2H).  $^{13}\text{C}$  NMR ( $\text{CDCl}_3$ ): d 171.2, 154.2, 149.6, 139.1, 136.7, 136.2, 136.1, 135.0, 131.9, 127.9, 127.5, 126.6, 126.5, 124.9, 124.0, 123.9, 122.2

$[\text{1H}]^+_4[\text{Fe}_2(\text{SCN})_{10}]^{4-}$  (**2**). **1** (0.11 g, 0.34 mmol) was dissolved in methanol (10 mL) and the solution was sparged with  $\text{N}_2$  gas for 10 min.  $\text{FeCl}_2 \cdot 4\text{H}_2\text{O}$  (0.021 g, 0.17 mmol) and NaSCN (0.027 g, 0.34 mmol) were added as solids and the mixture was heated to reflux for 96 h under an atmosphere of  $\text{N}_2$  and the solution turned dark purple over this time. The solution was rotovaped to dryness to produce a crude dark solid. The crude solid (3–4 mg batches) was recrystallized by dissolution into  $\text{CH}_2\text{Cl}_2$  and layering hexanes on top carefully (in a ratio of 1:2). Dark violet needle crystals suitable for X-ray diffraction formed

within 24 h. Yield, 20 mg. Calculated for  $\text{C}_{78}\text{H}_{48}\text{N}_{14}\text{S}_{22}\text{Fe}_2$  (found): C, 46.9 (46.1); H, 2.4 (2.4); N, 9.8 (9.2%). HR-MS (ESI+): Calc'd for  $\text{C}_{17}\text{H}_{12}\text{NS}_3\text{C}$   $m/z$  326.0126  $[\text{MH}^+]$ , found 326.0124. FT-IR (KBr): 3237 (w), 3094 (w), 2110 (w), 2069 (m sh), 2035 (s), 2021 (m sh), 1618 (w), 1599 (w), 1281 (w), 1229 (w), 1045 (w), 827 (w), 770 (w), 700 (m)  $\text{cm}^{-1}$ . UV-Vis ( $\text{CH}_2\text{Cl}_2$ ),  $\lambda_{\text{max}}$  ( $\epsilon$   $\text{M}^{-1} \text{cm}^{-1}$ ): 331 ( $7.4 \times 10^3$ ), 508 ( $5.3 \times 10^3$ ), 560 (sh,  $4.1 \times 10^3$ ).

## Results and discussion

### Synthesis and structural properties

Ligand **1** was synthesized in three steps from commercially available 3-bromothiophene. Bromination of 3-bromothiophene with  $\text{HBr}/\text{Br}_2$  produced 2,3,5-tribromothiophene, which was subjected to Suzuki-Miyura cross-coupling conditions to yield 3'-bromo-2,2':5',2''-terthiophene. The final step in the preparation of **1** was a Negishi cross-coupling of 3'-bromo-2,2':5',2''-terthiophene with 2-pyridylzinc bromide. There is one other report that describes the preparation of **1**, via Stille cross-coupling methodology but our method has the advantage of not having to use toxic organotin reagents. Reacting two equivalents of **1** with " $\text{Fe}(\text{NCS})_2$ ", prepared in situ by reaction between hydrated  $\text{FeCl}_2$  and NaSCN, in methanol produced not the anticipated  $(\text{1})_2\text{Fe}(\text{NCS})_2$ , where **1** is binding to the ferrous ion in a bidentate manner, through pyridyl N and terminal thiophene ring S donor atoms. Rather, a deep purple powder was isolated, which produced violet needle crystals suitable for X-ray diffraction by layering hexanes on to a  $\text{CH}_2\text{Cl}_2$  solution of the powder. Single crystal X-ray diffraction revealed an unusual structure, consisting of a homoleptic bimetallic  $[\text{Fe}_2(\text{SCN})_{10}]^{4-}$  tetra-anion [containing iron(3+)] with charge balance provided by four equivalents of  $[\text{1H}]^+$  protonated at the pyridine N atom. It appears that the oxidation of the ferrous ions occurs over the course of the reaction since recrystallization in air or under an inert atmosphere produces the same ferric containing material. To our knowledge, this bimetallic iron(3+) thiocyanate complex represents the first structurally characterized ferric dimer featuring  $\mu$ -1,3-thiocyanato bridging ligands. In our literature search, we could only find two other reports of dimeric iron complexes with  $\mu$ -1,3-thiocyanato bridging ligands. These other reports include an iron(2+) dimer with macrocyclic ligands<sup>15</sup>, which was characterized with single crystal X-ray diffraction and a ferric dimer suspected to be of the form  $\text{K}_2[\text{Fe}_2(\text{SCN})_8]$ <sup>16</sup>, which was characterized without single crystal data nor variable temperature magnetic susceptibility data.

The molecular structure of **2** is shown in Figures 1–3. The four cations and tetra-anion are shown separately for clarity. Relevant metrical parameters are included in the figure captions. The tetra-anion includes a bimetallic iron(3+) unit with two bridging  $\mu$ -1,3-thiocyanato ligands. Each ferric ion is coordinated by one N- and one S-bound  $\mu$ -1,3-thiocyanato. The remaining four coordination sites at each metal are occupied by terminal N-bound thiocyanates, generating an unusual homoleptic  $\text{Fe-N}_5\text{S}$  coordination sphere at each metal ion. The  $\text{Fe-NCS}_{\text{terminal}}$  coordinate bond distances range from 1.974(6) to 2.048(7) Å. The Fe-N bond distances to the bridging thiocyanates are longer than the bonds to the terminal bound thiocyanate N atoms [2.088(7) and 2.084(6) Å]. The longest coordinate bonds are between Fe and S [2.680(2) and 2.676(2)

Å]. The distance between the Fe ions within the anion is 5.740 Å. Each coordinated thiocyanate is linear, with near ideal NCS bond angles ranging from 177.6(8) to 179.1(7) degrees. The bond angles that include Fe and the bridging S and N atoms [S(2)-Fe(1)-N(1) and S(1)-Fe(2)-N(2)], which are important for the transmission of any intramolecular magnetic exchange coupling between the metal ions, are 88.37(18) and 87.99(18) degrees, respectively. To our knowledge and surprise, **2** represents the first bimetallic iron(3+) complex with bridging  $\mu$ -1,3-thiocyanate ligands characterized by X-ray crystallography. We found one report containing single crystal X-ray diffraction data for a bimetallic ferrous complex with the same bridge structure from Wieghardt and co-workers.<sup>15</sup> In this complex, the Fe-N [2.14(2)] bond distances to the bridging thiocyanate anions are significantly longer than the same distances in **2** [2.088(7) and 2.084(6)], which is consistent with the ferric oxidation state assignment in **2**.

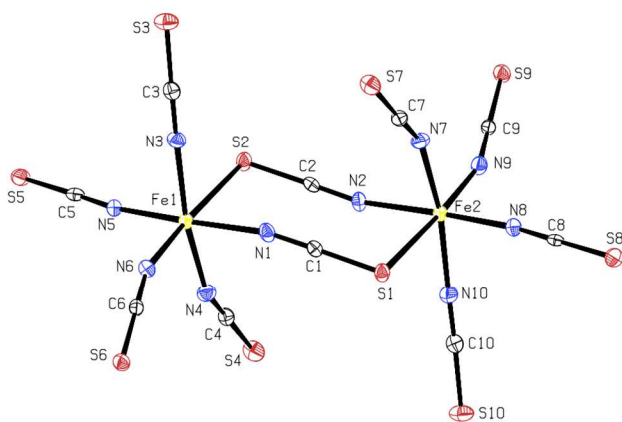


Fig. 1. Molecular structure of the tetra-anion of **2** (displacement ellipsoids at 30% probability). Relevant bond distances (Å) and angles (°) [with standard uncertainties (su) in brackets]: Fe(1)-N(5), 1.974(6); Fe(1)-N(6), 2.020(7), Fe(1)-N(4), 2.039(7); Fe(1)-N(3), 2.040(7); Fe(1)-N(1), 2.088(7); Fe(1)-S(2), 2.680(2); Fe(2)-N(8), 1.989(6); Fe(2)-N(9), 2.033(7); Fe(2)-N(10), 2.046(7); Fe(2)-N(7), 2.048(7); Fe(2)-N(2), 2.084(6), Fe(2)-S(1), 2.676(2); S(1)-C(1), 1.637(8); S(2)-C(2), 1.638(8); S(3)-C(3), 1.629(8); S(4)-C(4), 1.617(8); S(5)-C(5), 1.596(8); S(6)-C(6), 1.607(8); S(7)-C(7), 1.616(8); S(8)-C(8), 1.598(8); S(9)-C(9), 1.606(8); S(10)-C(10), 1.631(8); N(1)-C(1), 1.161(10); N(2)-C(2), 1.160(10); N(3)-C(3), 1.157(10); N(4)-C(4), 1.172(10); N(5)-C(5), 1.179(10); N(6)-C(6), 1.183(10); N(7)-C(7), 1.172(10); N(8)-C(8), 1.173(10); N(9)-C(9), 1.170(10); N(10)-C(10), 1.146(10). N(5)-Fe(1)-N(6), 97.0(3); N(5)-Fe(1)-N(4), 89.3; N(6)-Fe(1)-N(4), 94.6(3); N(5)-Fe(1)-N(3), 90.9(3); N(6)-Fe(1)-N(3), 96.8(3); N(4)-Fe(1)-N(3), 168.3(3); N(5)-Fe(1)-N(1), 174.1(3); N(6)-Fe(1)-N(1), 88.6(3); N(4)-Fe(1)-N(1), 88.0(3); N(3)-Fe(1)-N(1), 90.1(3); N(5)-Fe(1)-S(2), 85.95(19); N(6)-Fe(1)-S(2), 176.5(2); N(4)-Fe(1)-S(2), 83.6(2); N(3)-Fe(1)-S(2), 84.88(19); N(1)-Fe(1)-S(2), 88.37(18); N(8)-Fe(2)-N(9), 96.7(3); N(8)-Fe(2)-N(10), 90.5(3); N(9)-Fe(2)-N(10), 96.9(3); N(8)-Fe(2)-N(7), 90.5(3); N(9)-Fe(2)-N(7), 94.8(3); N(10)-Fe(2)-N(7), 168.0(3); N(8)-Fe(2)-N(2), 174.7(3); N(9)-Fe(2)-N(2), 88.5(3); N(10)-Fe(2)-N(2), 89.8(3); N(7)-Fe(2)-N(2), 88.1(3); N(8)-Fe(2)-S(1), 86.8(2); N(9)-Fe(2)-S(1), 176.18(19); N(10)-Fe(2)-S(1), 84.5(2); N(7)-Fe(2)-S(1), 83.6(2); N(2)-Fe(2)-S(1), 87.99(18).

The molecular structure of **2** also contains four crystallographically independent cations of protonated **1** in the asymmetric unit (one of the cations is shown in Figure 2 and the other three cations of protonated **1** are presented in the Supporting Information as Figures S1-S3). In each cation, the 2-pyridyl substituent is protonated at N and each N-H acts as a hydrogen bond donor to S atoms of the anion dimer. In two of the cations, two of the thiophene rings are disordered, and in the other two cations, only one thiophene ring is disordered.

The disorder in all instances is the result of rotation of the ring by approximately 180 degrees. The bond distances and angles for each of the cations are very similar to each other and typical for other similar molecules of this type. It is likely that the protonation of **1** occurred in the coordination reaction from the  $\text{H}_3\text{O}^+$  produced from the dissolved  $\text{FeCl}_2 \cdot 4\text{H}_2\text{O}$  (which may or may not have been oxidized), which is a weak aqua acid with a  $K_a$  on the order of  $10^{-9}$ . Alternatively, a protic solvent (methanol) was used in the preparation of **2**.

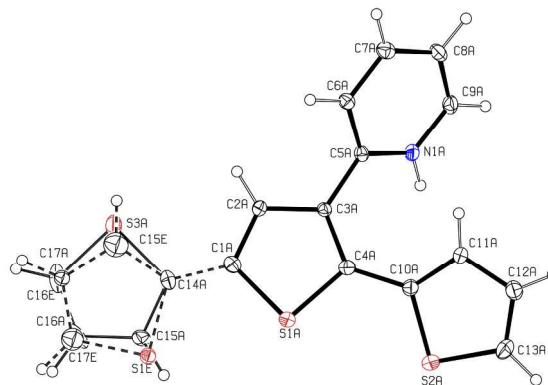


Fig. 2. Molecular structure of the protonated cation of **2** (one of four protonated cations in the asymmetric unit is shown for clarity). Displacement ellipsoids at 30% probability (su values in brackets) and the dashed lines indicate a minor component of disorder. Relevant bond distances (Å) and angles (°): S(1A)-C(4A), 1.732(8); S(1A)-C(1A), 1.732(8); N(1A)-C(5A), 1.346(9); N(1A)-C(9A), 1.347(10); C(1A)-C(2A), 1.367(10); C(1A)-C(14A), 1.454(9); C(2A)-C(3A), 1.420(10); C(3A)-C(4A), 1.387(10); C(3A)-C(5A), 1.463(9); C(4A)-C(10A), 1.469(9); C(5A)-C(6A), 1.385(10); C(6A)-C(7A), 1.390(10); C(7A)-C(8A), 1.388(12); C(8A)-C(9A), 1.361(12); S(2A)-C(13A), 1.702(6); S(2A)-C(10A), 1.712(5); C(10A)-C(11A), 1.385(6); C(11A)-C(12A), 1.403(7); C(12A)-C(13A), 1.351(6); S(3A)-C(17A), 1.699(7); S(3A)-C(14A), 1.713(5); C(14A)-C(15A), 1.387(7); C(15A)-C(16A), 1.398(8); C(16A)-C(17A), 1.350(7); S(1E)-C(17E), 1.705(8); C(15E)-C(16E), 1.401(8); C(16E)-C(17E), 1.352(7). C(4A)-S(1A)-C(1A), 93.0(4); C(5A)-N(1A)-C(9A), 123.3(7); C(2A)-C(1A)-C(14A), 128.3(7); C(2A)-C(1A)-S(1A), 110.3(6); C(14A)-C(1A)-S(1A), 121.4(5); C(1A)-C(2A)-C(3A), 113.8(7); C(4A)-C(3A)-C(2A), 113.0(6); C(4A)-C(3A)-C(5A), 125.0(7); C(2A)-C(3A)-C(5A), 122.0(6); C(3A)-C(4A)-C(10A), 130.1(6); C(3A)-C(4A)-S(1A), 109.9(6); C(10A)-C(4A)-S(1A), 120.0(5); N(1A)-C(5A)-C(6A), 118.1(6); N(1A)-C(5A)-C(3A), 119.9(6); C(5A)-C(6A)-C(7A), 119.8(7); C(8A)-C(7A)-C(6A), 119.7(7); C(9A)-C(8A)-C(7A), 119.2(7); N(1A)-C(9A)-C(8A), 119.9(7).

The molecular packing of **2** in the *ab* plane is also shown in Figure 3. No close intermolecular contacts could be found for the tetra-anion, which contains the paramagnetic ferric ions. As a result, the variable temperature magnetic properties of **2** should be those of a well-isolated ferric dimer.

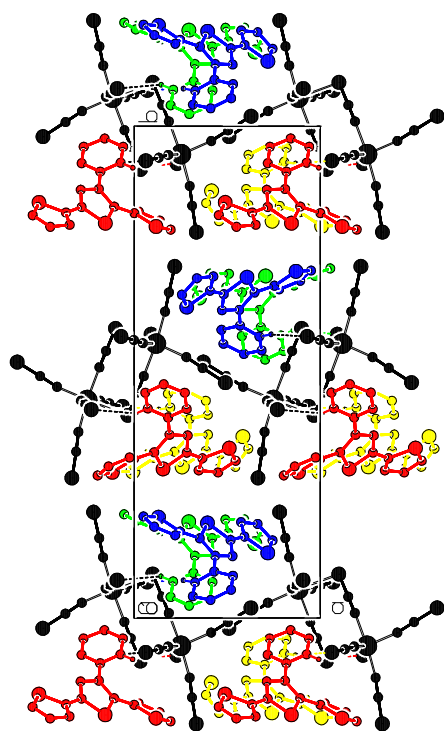


Fig. 3. Molecular packing of **2** in the *ab* plane. **2** is indicated in black and the four crystallographically independent cations of  $[1H]^+$  are colored red, yellow, green, and blue. **Crystal data.**  $C_{78}H_{48}Fe_2N_{14}S_{22}$ ,  $M = 1998.32$ , monoclinic,  $a = 11.6864(4)$ ,  $b = 29.2257(9)$ ,  $c = 13.0996(4)$  Å,  $U = 4233.9(2)$  Å<sup>3</sup>,  $T = 147(2)$  K, space group  $P_{21}$ ,  $Z = 2$ , 84784 reflections measured, 14940 unique ( $R_{int} = 0.0652$ ) which were used in all calculations. The final  $wR(F_2)$  was 0.1095 (all data).

### Spectroscopic and electronic properties

The FT-IR spectrum of **2** is dominated by the CN stretching absorptions over the range 2150–1950  $cm^{-1}$ , as anticipated for this structure (Figure S4 in the Supporting Information). The higher energy absorptions in this region are assigned to the CN stretching frequencies of the bridging thiocyanates, as has been observed previously. The terminal thiocyanates absorb at slightly lower energy. Other absorptions from  $[1H]^+$  are also present in the spectrum.

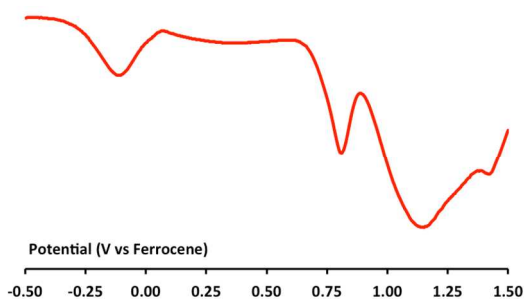


Fig. 4. Differential pulse voltammogram of **2** in  $CH_2Cl_2$  (versus ferrocene) containing approximately 0.5 M  $Bu_4NPF_6$  (scan rate 25 mV/sec)

Apart from the single crystal X-ray diffraction data, evidence for the ferric oxidation state in **2** is provided by the differential pulse (DP) voltammogram (Figure 4). A low potential cathodic wave is observed (the only cathodic process of note), which is ascribed to the reduction of ferric ions (the reduction of each

ion occurs simultaneously, as is typical when there is only very weak electronic coupling between the ions). Anodic processes at +0.8 and +1.1 V (versus ferrocene) can be attributed to oxidations of coordinated thiocyanate and the terthienyl cation, respectively.

The UV-visible spectrum of **2** was also measured in  $CH_2Cl_2$  solution (Figure 5). A low energy absorptions at 508 nm with a slightly lower energy shoulder (557 nm) can be assigned as thiocyanate-to-iron(3+) charge transfer (LMCT) on the basis of the molar absorptivity values ( $5.3 \times 10^3$  and  $4.2 \times 10^3$   $M^{-1} cm^{-1}$ ). No weak d-d transitions could be detected in concentrated solutions, which provides further evidence for the high-spin ferric oxidation assignments. High energy absorptions (320 nm and lower) are likely  $\pi-\pi^*$  transitions within  $[1H]^+$ .

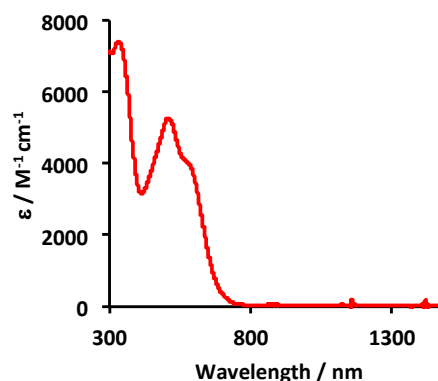


Fig. 5. UV-visible-NIR spectrum of **2** recorded in  $CH_2Cl_2$  at 298K.

### Variable temperature magnetic susceptibility

The variable temperature magnetic susceptibility properties of **2** were investigated with a superconducting quantum interference device (SQUID) over a temperature range of 300 to 2 K. Single crystals of **2** were carefully harvested from recrystallization experiments and these crystals were ground and the pulverized material was placed in gel caps. As previously noted, the lack of any significant close intermolecular contacts between the tetra-anions in **2** from the single crystal X-ray diffraction data suggest any temperature dependent magnetic phenomenon observed will be largely the result of intramolecular magnetic exchange coupling between the ferric ions through the thiocyanate bridging ligands. The variable temperature magnetic properties of **2** are shown in Figure 6 as plots of  $\chi_m T$  or  $\chi_m$  versus  $T$ . The room temperature value of  $\chi_m T$  is 8.2  $cm^3 K mol^{-1}$ , which is a little less than the anticipated value (8.75  $cm^3 K mol^{-1}$ ) for two uncoupled ferric ions ( $g = 2$ ) in the absence of any temperature independent paramagnetism (TIP). With decreasing temperature, however, there is a steady decrease in  $\chi_m T$  as anticipated for intramolecular antiferromagnetic magnetic coupling interactions between the metal ions. The value of  $\chi_m T$  at 2 K is 0.5  $cm^3 K mol^{-1}$ , suggesting an  $S = 0$  ground state for **2**. The plot of  $\chi_m$  versus  $T$  displays a maximum in  $\chi_m$  at low temperature, as is typically observed in antiferromagnetically coupled dimers. In fact, we can very nicely fit the experimental susceptibility data to a simple ferric dimer isotropic spin Hamiltonian model of the form

$$\hat{H} = 2JS_{Fe}S_{Fe}$$

which provides the following best fit parameters:  $J = -4 \text{ cm}^{-1}$ ,  $g = 2.04$ ,  $\theta = -1 \text{ K}$ ,  $\rho = 0.03$ . The profile of the  $\chi_m T$  data and the  $\chi_m$  maximum at low temperature indicate a weak antiferromagnetic interaction between the ferric ions in the complex. A magnetization versus field experiments at 2 K confirms the  $S = 0$  ground state in **2** (Figure S5 in the Supporting Information).

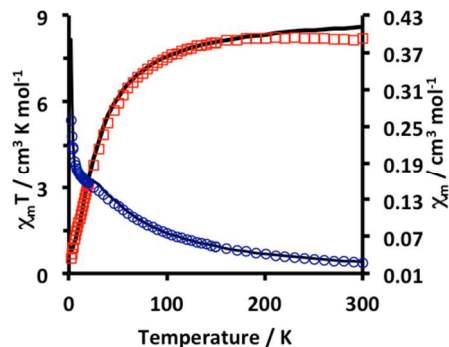


Fig. 6. Variable temperature magnetic susceptibility of **2** shown as plots of  $\chi_m T$  vs  $T$  (red squares) or  $\chi_m$  vs  $T$  (blue circles) at an external field of 2000 Oe. Black solid lines represent best fits to the experimental data using the spin Hamiltonian and best-fit parameters described in the text.

### Density functional theory (DFT) calculations

Using the coordinates from the X-ray diffraction data, we calculated the single point energy of the high-spin ( $S = 5$ ) and Broken symmetry (BS)<sup>17</sup> states of the tetra-anion component of **2** using the B3LYP functional with the def2-TZVP basis set on all atoms. The energy of the BS state was found to be very slightly lower than the high spin state ( $\Delta E = 106 \text{ cm}^{-1}$ ). The energy of the closed-shell singlet state was found to be much higher ( $\Delta E = 2.9 \times 10^4 \text{ cm}^{-1}$ ). Using the approach of Yamaguchi<sup>18</sup>, we could calculate the magnetic exchange coupling constant from the energies of the high spin (HS) or BS wavefunctions and their spin expectation values as follows

$$2J = -\frac{(E_{HS} - E_{BS})}{\langle S^2 \rangle_{HS} - \langle S^2 \rangle_{BS}}$$

This procedure provides a calculated magnetic exchange value of about  $-4 \text{ cm}^{-1}$ , which is identical to the fitted value obtained from the variable temperature magnetic susceptibility data. To rationalize the weak exchange coupling we computed the spin density distribution (Figure 7) in the tetra-anion of **2** and found most of the spin density localized on the ferric ions, with very little delocalization onto the bridging thiocyanates (this is likely the main superexchange pathway for any magnetic communication in this complex)

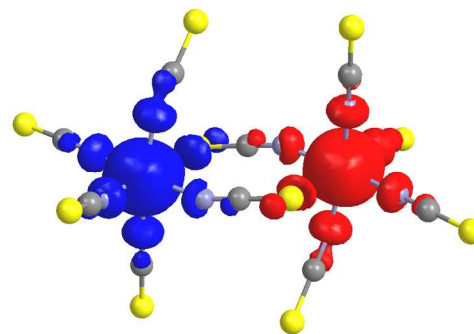


Fig. 7. Spin density distribution in the tetra-anion component of **2** (def2-TZVP/B3LYP). Isovalue 0.004.

### Conclusions

In summary, we have reported the structural and magnetic properties of the first bimetallic  $\mu$ -1,3-bis(thiocyanato)-bridged ferric complex. The structural data indicate a very unusual and completely homoleptic tetra-anion featuring two ferric ions and include both bridging and monodentate thiocyanate ligands. The paramagnetic anionic components are well isolated among layers of organic cations and this is reflected in the variable temperature magnetic susceptibility data, which indicates weak intramolecular antiferromagnetic exchange coupling between the high-spin ferric ions. The magnetic data could be fit well to a  $S = 5/2$  dimer model. DFT calculations on the tetra-anion component of the complex support the weak antiferromagnetic exchange coupling with the spin density mainly localized on the ferric ions with little delocalization onto the bridging ligands.

### Acknowledgements

MTL thanks NSERC (Discovery), CFI, Canada Research Chairs program and Brandon University for funding. Dr. Paul Dube (Brockhouse Institute for Materials Research) and Prof. Fereidoon Razavi (Brock University) are thanked for providing variable temperature magnetic susceptibility data.

### Notes and references

<sup>a</sup> Department of Chemistry, Brandon University, Brandon, MB, R7A 6A9, CANADA.

<sup>b</sup> Department of Chemistry, University of Toronto, Toronto, ON, M1S 3H6, CANADA.

Electronic Supplementary Information (ESI) available: Displacement ellipsoid plots of other crystallographically independent  $[\text{1H}]^+$  cations, magnetization versus field data for **2** and crystallographic data for **2** in cif format. See DOI: 10.1039/b000000x/

- 1 B. Machura, A. Switlicka, J. Mrozinski, B. Kalinska and R. Kruszynski, *Polyhedron*, 2013, **52**, 1276.
- 2 T. Rojo, R. Cortés, L. Lezama, M. I. Arriortua, K. Urriaga and G. Villeneuve, *Dalton Trans.* 1991, 1779.
- 3 R. Vincente, A. Escuer, J. Ribas and X. Solans, *Dalton Trans.* 1994, 259.
- 4 M. Monfort, J. Ribas and X. Solans, *Inorg. Chem.* **1994**, *33*, 4271.

## ARTICLE

- 5 A. Escuer, R. Vincente, M. S. El Fallah, X. Solans and M. Font-Bardia, *Dalton Trans.* 1996, 1013.
- 6 J. A. R. Navarro, M. A. Romero, J. M. Salas, M. Quirós and E. R. T. Tiekink, *Inorg. Chem.* **36**, 4988.
- 7 B. Djukic, S. I. Gorelsky, A. J. Lough and M. T. Lemaire, *Inorg. Chem.* 2011, **50**, 7334.
- 8 M. O. Wolf, *Adv. Mater.* 2001, 13, 545.
- 9 C. Dragonetti, S. Righetto, D. Roberto, A. Valore, T. Benincori, F. Sannicolò, F. De Angelis and S. Fantacci, *J. Mater. Sci.: Mater. Electron.*, 2009, **20**, S460.
- 10 Gaussian 09, Revision D.01, M. J. Frisch, G. W. Trucks, H. B. Schlegel, G. E. Scuseria, M. A. Robb, J. R. Cheeseman, G. Scalmani, V. Barone, B. Mennucci, G. A. Petersson, H. Nakatsuji, M. Caricato, X. Li, H. P. Hratchian, A. F. Izmaylov, J. Bloino, G. Zheng, J. L. Sonnenberg, M. Hada, M. Ehara, K. Toyota, R. Fukuda, J. Hasegawa, M. Ishida, T. Nakajima, Y. Honda, O. Kitao, H. Nakai, T. Vreven, J. A. Montgomery, Jr., J. E. Peralta, F. Ogliaro, M. Bearpark, J. J. Heyd, E. Brothers, K. N. Kudin, V. N. Staroverov, R. Kobayashi, J. Normand, K. Raghavachari, A. Rendell, J. C. Burant, S. S. Iyengar, J. Tomasi, M. Cossi, N. Rega, J. M. Millam, M. Klene, J. E. Knox, J. B. Cross, V. Bakken, C. Adamo, J. Jaramillo, R. Gomperts, R. E. Stratmann, O. Yazyev, A. J. Austin, R. Cammi, C. Pomelli, J. W. Ochterski, R. L. Martin, K. Morokuma, V. G. Zakrzewski, G. A. Voth, P. Salvador, J. J. Dannenberg, S. Dapprich, A. D. Daniels, Ö. Farkas, J. B. Foresman, J. V. Ortiz, J. Cioslowski, and D. J. Fox, Gaussian, Inc., Wallingford CT, 2009.
- 11 A. D. Becke, *J. Chem. Phys.* 1993, **98**, 5648.
- 12 C. Lee, W. Yang and R. G. Parr, *Phys. Rev.* 1988, **B37**, 785.
- 13 F. Weigend and R. Ahlrichs, *Phys. Chem. Chem. Phys.* 2005, **7**, 3297.
- 14 L. V. Skripnikov, Chemissian V. 4.01, Visualization Computer Program, [www.chemissian.com](http://www.chemissian.com), 2014.
- 15 K. Pohl, K. Wieghardt, B. Nuber and J. Weiss, *Dalton Trans.* 1987, 187.
- 16 S. Gerber, H. Krautscheid, T. Gelbrich and H. Vollmer, *Z. Anorg. Allg. Chem.* 2004, **630**, 1427.
- 17 L. Noodleman, *J. Chem. Phys.* 1979, **74**, 5737.
- 18 H. Nagao, M. Nishino, Y. Shigeta, T. Soda, Y. Kitagawa, T. Onishi, Y. Yoshioka and K. Yamaguchi, *Coord. Chem. Rev.* 2000, **198**, 265.